Surface Review and Letters
© World Scientific Publishing Company

ELECTRONIC AND OPTICAL MODIFICATION OF ORGANIC-2D PEROVSKITES

SILMI KAFFAH
Department of Computer Systems Engineering, Prasetiya Mulya University, Kavling Edutown I.1, Jl. BSD Raya Utama, BSD City
Tangerang 15339, Indonesia
silmi.kaffah@prasetiyamulya.ac.id

LINA JAYA DIGUNA
Department of Renewable Energy Engineering, Prasetiya Mulya University, Kavling Edutown I.1, Jl. BSD Raya Utama, BSD City
Tangerang 15339, Indonesia
lina.diguna@prasetiyamulya.ac.id

ABU BAKAR SURIANI
Nanotechnology Research Centre, Faculty of Science and Mathematics, Universiti Pendidikan Sultan Idris
35900 Tanjung Malim, Perak, Malaysia
suriani@fsmt.upsi.edu.my

ARRAMEL
Group, Company, Address
City, State ZIP/Zone, Singapore
phyarr@nus.edu.sg

DANANG BIROWOSUTO
Department of Renewable Energy Engineering, Prasetiya Mulya University, Kavling Edutown I.1, Jl. BSD Raya Utama, BSD City
Tangerang 15339, Indonesia
muhammad.birowosuto@prasetiyamulya.ac.id

Received (Day Month Year)

The abstract should summarize the context, content and conclusions of the paper. It should not contain any references or displayed equations. Typeset the abstract in 9 pt Times Roman with baselineskip of 11 pt, making an indentation of 2.5 picas on the left and right margins.

Keywords: X-ray and ultraviolet photoelectron spectroscopy; hybrid organic-inorganic perovskite; energy level alignment.

1. Introduction

Two-dimensional hybrid organic-inorganic perovskites (2D-HOIPs) have emerged to the surface as viable alternatives to three-dimensional hybrid organic-inorganic perovskites (3D-HOIPs) solar cells absorbers such as $MAPbI_3$ (MA = methylammonium) and other related family.[1–8] The current

reports in this fields indicated that the optoelectronic devices using 3D hybrid-based perovskite has a tradeoff concerning their stability. For example, the moisture instability, halide vacancies, ion migration, and interstitials have hampered its progress as an alternative of silicon.[9,10] In comparison to the 3D analogues, 2D-HOIPs have an improved processability and stability towards water and light.[11–13] These could originate from the fact that the hydrophobic nature of the organic cations in 2D perovskites that replace the volatile and hydrophilic methylammonium in 3D perovskite could serve as a protective layer from the harsh environment.

In terms of the advancement of the structural diversity in hybrid perovskites, 2D-HOIPs have evolved their progress into vast collection of examples with compelling chemical composition and multiple platforms. In recent years, diverse classes of hybrid perovskites have been investigated extensively. Several comprehensive reviews illustrated the structural guidelines of the reduced dimensionality perovskites, focusing on 2D-perovskite derivatives which hold promise in their tunability and excellent photophysical properties. For example, these materials can be considered as quantum wells in which the semiconducting inorganic sheets are separated by the insulating organic barriers.[7,14,15] In this review, we mention several member of the groups that essentially can be classified into three categories based on the coordination nature of the inorganic layers and its connectivity with the insulating organic moiety barrier. These structural model can be rationalized based on the the cleavage direction along the $\langle 100 \rangle$, $\langle 110 \rangle$, and $\langle 111 \rangle$ crystallographic planes of the parent 3D hybrid perovskite structure. The most rich database in the literature focuses on the $\langle 100 \rangle$-oriented perovskites.[4,16,17] Depending on the viable choice of the capping cation and relative position between the inorganic sheets, this material can be classified further into three categories: Aurivillius phase,[18] Dion-Jacobson (DJ) phase,[19,20] and Ruddlesden-Popper (RP) phase.[3,4,21] The latter one can be ascribed as a slab that interleaved with cations generally found in the halide perovskites family.[4,22] The general chemical formula of $L_2A_{n-1}B_nX_{3n+1}$, where L represents a large cation, A is a small cation (for example Caesium and MA^+), B is a divalent metal cation (Pb^{2+} and Sn^{2+}) and X is a halide. The large variety of such hybrid perovskites promote a fine tuning of their photophysical and electronic properties across solar cells, light-emitting diodes, and field effect transistor applications. Further description on the structure-property relationship of these emergent 2D materials have been comprehensively described elsewhere.[1–8]

This review summarizes recent literature on the role of organic semiconductors as the electronic dopants and trap passivation agents of hybrid perovskite absorbers, and their corresponding heterointerfaces are illustrated in Fig. 1. In particular, Section 2 includes a short discussion on the basic principles of the interfacial nature of perovskite absorbers and photoemission technique as surface-sensitive to analyze the chemical and electronic properties of 2D-HOIPs surfaces and interfaces. We next continue by reviewing recent developments on the application of organic molecules to engineering the interfacial electronic structure of 2D-HOIPs. In Section 3, we review recent progress in the perspective of tailoring the optical properties of 2D-HOIPs upon the addition of molecular materials. Section 4 summarizes the defect passivation strategy to enhance the performance of photovoltaics and light-emitting diodes. In the end, Section 5 includes a summary and perspectives.

2. Turning the Knob of Electrical Control in Organic-2D Perovskites Heterointerfaces

In a similar fashion as the conventional semiconductor crystals, several types of defects in ABX_3 perovskite system are commonly identified from the intrinsic to extrinsic surface defects. The surrounding environment or unsaturated surface bonds can be detrimental factor in determining hybrid perovskite as active material in solar-based devices. Theoretically, Yin et al. postulated three possible intrinsic point defects across $MAPbI_3$.[29] Namely, the atomic constituent vacancies (MA/Pb/I), interstitial (I interstitials (I_i) or MA interstitials (MA_i) substitution. The third case covers anti-site substitutions (MA-on-Pb substitutions (MA_{Pb}), Pb-on-MA substitutions (Pb_{MA}), and MA-on-I substitutions (MA_I)). These defects sites exhibit very shallow transition energy levels near the band edges.[29,30] On the other hand, the implication of chemical composition within the $MAPbI_3$ led to deep-level defects, such as I-on-MA substitutions (I_{MA}), Pb-on-I substitutions

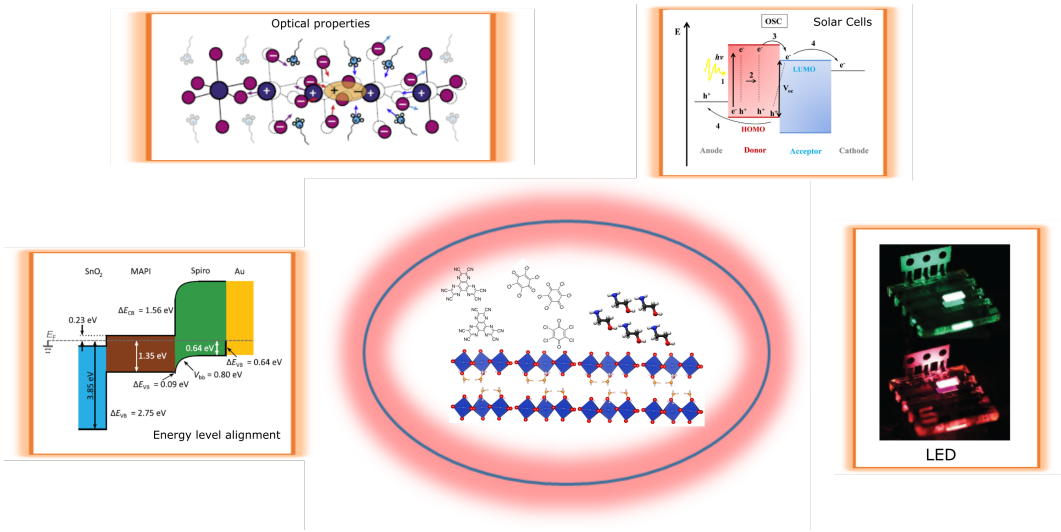

Fig. 1.: Schematic illustration of the organic molecule/2D-HOIPs heterointerfaces and their practical applications. The energy level alignment is adapted from Ref.[23] The exciton representation is adapted from Ref.[24] The charge carriers collection processes is adapted from Ref.[25] The green and red electroluminescence devices are adapted from Ref.[26]

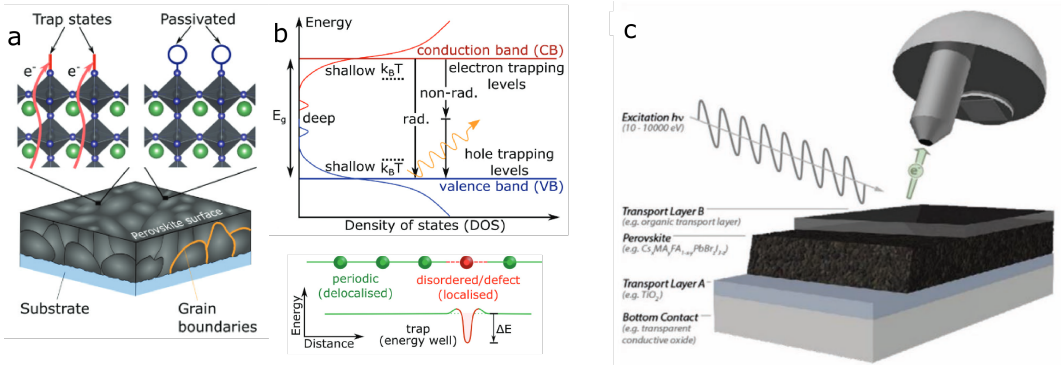

Fig. 2.: (a) Schematic illustration of parasitic recombination at surface traps (and subsurface traps) being passivated by introducing additional atoms/molecules (blue circle) which binds to improperly bound orbitals resulted the presence of trap states. (b) top panel, representation of state density in a disordered semiconductor, whereby both band-to-band radiative (rad.) and non-band-to-band non-radiative (non-rad.) recombination (vertical arrows) can occur. Bottom panel outlines the charge localization driven by non-periodic disorder and defect in a semiconductor lattice which introduce new energetic levels. Reproduced with permission from Ref.[27] (c) Photoemission spectroscopy of halide perovskite thin films on top of a transport layer. Reproduced with permission from Ref.[28]

(Pb_I), I-on-Pb substitutions (I_{Pb}) and Pb interstitials (Pb_i), have high formation energies. These in turn are responsible for the existence of the non-radiative recombination centers in perovskite under Pb-poor (I-rich) or Pb-rich (I-poor) conditions.[31–33]

In the case of 2D layered hybrid perovskites, the origin of such inefficient radiative recombination is not yet fully understood. The presence of fast exciton quenching at room temperature led to high trap density that promote such undesired event.[15,34,35] To shed some light in this subject,

Liu et al. discussed the defect properties and carrier recombination dynamics of the $BA_2MA_3Pb_4I_{13}$ perovskite film and device. It turns out that the defects in 2D perovskite are mainly governed by the deep level defects with an activation energy (E_a) of 0.398 eV, which is much higher than that of 3D perovskite (0.075 eV).[36] In the theoretical perspective, Ghosh et al. describes that the nonradiative carrier recombination processes greatly influenced by the electron-phonon interactions mediated from the structural fluctuations and instantaneous charge localization in the RP and DJ phases two-dimensional halide perovskite materials.[37] Several interesting reviews summarized the current understanding of the morphology and electronic structure of defects across hybrid perovskite materials at atomic-level resolution using versatile technique such as scanning probe microscopy.[38–40] Based on these aforementioned examples, the current advancement of the 2D-HOIPs research is mostly oriented to tailor their diverse chemical composition towards the realization of hybrid-based devices with better moisture and illumination stability.

A closer topological impact of the solution-processed hybrid perovskites thin films is mainly dominated by the grainy and polycrystalline networks of the surface. Thus, it creates surface imperfections such as intrinsic (or native) point defects that promote the charge carrier entrapment, thereby reducing the device performance. For example, Fig. 2a shows the implication of halogen-terminating surface establish undesired traps driven caused by the lack of local stoichiometric composition and improper surface bonding (left), which can be solved by introducing the so called passivator (i.e. surface chemical treatment). In order to acquire an effective passivation treatment (indicated by the blue circle), chemical bonds is interfaced at the Pb-X derived surface orbitals using molecular adlayer that shift the defect level either toward or into the band edges, minimizing the negative impact of such defect. Further comprehensive description on the nature of trap discussion can be found in the recent excellent reviews.[27,41–44]

In Fig. 2b (top panel), a representative energy scheme illustrate the relative energetic position of shallow traps that has a relatively small difference in energy with respect to their conduction/valence band edges ($\Delta E \leq k_B T$), while deep traps reside in the middle of the semiconductor bandgap ($\Delta E \geq k_B T$). Typically, shallow traps will only restrict the free charges movement through trapping and detrapping processes, while deep traps hinder detrapping and they facilitate the non-radiative recombination pathways. As a result, the imperfections led to localized electronic states at energy levels which are different than the carrier transport bands, promoting for (photo-)generated free carriers to energetically fall into this undesired site (Fig. 2b, bottom panel).

The current challenges of 2D-HOIPs solar cell investigation mainly involve the interplay between the hysteresis effect and long-term stability. It turns out that they are found to be closely related to the quality of the corresponding surfaces by taking into account the atomically smooth interfaces. A convenient and powerful technique to probe the chemical state and electronic properties of surfaces and interfaces of 2D-HOIPs is using photoemission spectroscopy (PES) technique. Since the hybrid compounds comprise of different elements, then it is of importance to assess their chemical state to characterize their energetic band offsets upon interfacing with the other solar cell components such as hole/electron transporting layers. In a nutshell, PES can be approximated as a nondestructive analytical surface characterization on diverse materials based on the well-known photoelectric effect.[?,45,46]

In general, the experimental procedure is mainly performed under ultrahigh vacuum (UHV) condition with typical base pressure in the order of 10^{-10} mbar to 10^{-11} mbar as schematically shown in Fig. 2c. This surface-sensitive technique is versatile to determine the chemical state of specific element according to their specific binding energy region. According to the classical approach, the surface sample is usually impinged with high energy photons (X-ray dual anode, a gas discharge lamp, laser excitation or a synchrotron radiation source) such that the electron-bounded to the nucleus are emitted toward the surface. Some of the photo-emitted electrons that are successfully escape with certain kinetic energies detected by the energy analyzer and those binding energy can be determined upon correction by the work function of spectrometer. Further description on the instrumentation and knowledge of general PES technique can be found elsewhere.[?,47]

Given the intrinsic nature of 2D-HOIPs, multiple components and the intrinsic softness of organic spacer could be quite complex and result in poor electrical conductivity (charging) or (photo)chemical instabilities.[47–49] In addition, de-excitations and charge compensations are considerably quite challenging for the PES experiment. In a recent review, Béchu et al. illustrates a comprehensive summary that cover several factors to acquire an accurate PES measurement on these metal halide perovskites system.[28] These photoelectron-based studies comprise of X-ray (XPS),[50–52] ultraviolet (UPS),[51,53–55] inverse (IPES),[55,56] and angle-resolved (ARPES) photoemission spectroscopies. In addition, an extension mode of scanning probe technique so called Kelvin probe force microscopy (KPFM) based on the contact potential difference (CPD) is shortly discussed.

2.1. *The chemistry of energetic alignment processes at the interfaces between the hybrid-perovskites and molecular layers*

The emergence of hybrid organic-inorganic perovskite as an active layer for solar cells applications have greatly indebted to overcome several issues targeted a reliable device with high power conversion efficiency (PCE) performance. The underline question in this fields is how to obtain a good interfacial nature when the hybrid perovskite materials are intimately coupled onto charge carrier transporting layers or electrodes. Furthermore, the improvement on the charge separation and reduction of the undesired charge recombination would be the main interest toward the ideal energy level alignment (ELA) at the hybrid interfaces.[41,49,51,57–63] A simplified electron transfer that facilitate the charge carrier is feasible when the conduction band minimum (CBM) of perovskite materials should be higher than that of the electron transfer layers (e.g. TiO_2 or ZnO); and conversely, to facilitate hole transfer, the valence band minimum (VBM) of hybrid perovskite materials should be lower than that of hole transfer materials.[58] One should consider that a simplified energetic model with a perfect vacuum level alignment across the energy levels of perovskite and electron/hole transfer layers is not entirely true. This hypothesis interfacial states, interfacial dipoles and band bending could be influenced by the interplay between charge transfer and ionic migration at the perovskite interface. Thus, it might promote the Fermi level pinning between the two layers, and moreover the band onsets (or gap states) positions with respect to the vacuum level.

Earlier reviews have suggested that the full description of the energetic details to minimize the energy loss at the perovskite/charge transport layer heterointerfaces. Several initial cases in 3D-based hybrid perovskites heterointerfaces are formed with four possible profiles, namely, staggered gap (type I), straddling-gap (type II), reverse staggered-gap (type III) with the deep-lying of hole-transporting layer, and reverse straddling-gap heterointerface in contact with a HTM of large energy gap (Type IV).[57] For example, the energy differences between the perovskite VBM and the HTL's highest occupied molecular orbital (HOMO) (HOMO) determine the injection barrier or extraction barrier for holes. In other energy level, the energy differences between the perovskite CBM and the lowest unoccupied molecular orbital (LUMO) (LUMO) determine the injection barrier or extraction barrier for electrons. The former will limit the open circuit voltage (V_{OC}) due to thermionic loss for holes, while the latter strongly affect the fill factor (FF) with the negligible effect on V_{OC}.[64]

Schulz and coworker dated in 2014 provided a fundamental knowledge how to minimize the energy loss in the solar cell device, namely, a small energy mismatch of the electronic energy levels in the perovskite layer compared to those of the adjacent transport layers is essentially required.[65] Fig. 7a outlines the approximate energy diagram across a layer stack of hybrid perovskite incorporated between the electron collecting cathode (TiO_2) and organic-based HTL on top part of the device. In their finding, 2,2',7,7'-tetrakis-(N,N-di-p-methoxyphenylamine)-9,90-spirobi-fluorene(spiro MeOTAD) layer. A successful and efficient operational device is achieved with certain criteria in which electrons was extracted from the perovskite into the conduction band of TiO_2, whereas holes are distributed the HOMO of spiro-MeOTAD. In this work, a combination UPS and IPES is intended to extract the occupied states at the interface and resulted the

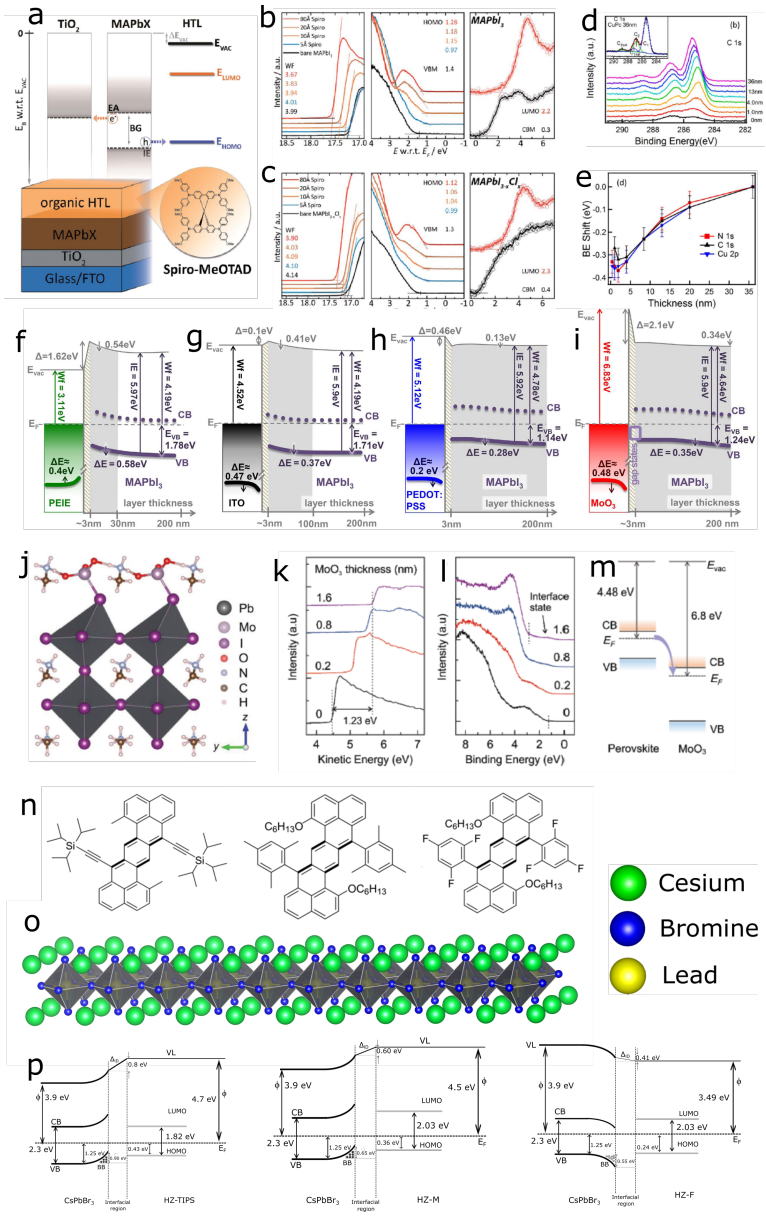

Fig. 3.: (a) Schematic of device structure and its corresponding energy diagram of a perovskite absorber (MAPbX)-based solar cell with an organic hole transport layer. Left panels: photoemission cut-off for the bare perovskite and as a function of hole transport layer (HTL) thickness, from which the vacuum level of the film is extracted. The occupied states evolution of $MAPbI_3$ (b) and $MAPbI_{3-x}Cl_x$ (c) upon the incremental change spiro-MeOTAD layers. The work functions of the bare perovskite films are in the range of 4.0 eV–4.1 eV. Middle panels: UPS spectra of the top of occupied states, i.e. VBM for the bare perovskites and HOMO for spiro-MeOTAD/perovskites as a function of HTL thickness. Right panels: IPES spectra of the bottom of unoccupied states of bare perovskites and 80 Å spiro-MeOTAD/perovskites. Reproduced with permission from Ref.[65] (d) The evolution of C1s core level spectra as the function of CuPc molecular thickness. (Inset) Detailed peak fitting of 36 nm CuPc film. (e) Binding energy shift of the three elements in CuPc film. Reproduced with permission from Ref.[66] Energetic alignment at the interfaces $MAPbI_3$ thin films on the four different substrates, namely (f) PEIE, (g) ITO, (h) PEDOT:PSS, and (i) MoO_3, respectively. Reproduced with permission from Ref.[67] (j) Relaxed geometric structure of the MoO_3-doped $MAPbI_3$ perovskite surface. (k) The secondary electron cut-off regime as a function of MoO_3 coverage. (l) Low binding energy region close to E_F. (m) Schematic energy level diagram depicted the electron transfer from perovskite to MoO_3. Reproduced with permission from Ref.[68] (n) Molecular structure of heptazethrenes derivatives HZ-TIPS (left), HZ-M (middle), and HZ-F (right). (o) Representation of cubic structure $CsPbBr_3$. Reproduced with permission from Ref.[69] (p) The corresponding energy band diagram across the heterointerface of the HZ-TIPS (left), HZ-M

WF determination as shown in the left panel of Figs. 7b ($MaPbI_3$) and 7c ($MAPbI_{3-x}Cl_x$), respectively. These findings suggested that the organic layer deposition does not change substantially the secondary electron cutoff, whereas for the $MAPbBr_3$ a downward vacuum level shift about 0.15 eV was observed at the interface. In terms of VBM region, for all the reported perovskite/organic heterointerface did not affect significantly. Interestingly, The IPES spectra yield CBM positions 0.3 eV above E_F in $MAPbI_3$ and 0.4 eV in $MAPbI_{3-x}Cl_x$ (Right panel, figures 7b and 7c). These values suggest that the perovskite CBM established a large barrier for electrons and therefore preventing any unwanted electron collection in that layer. In a similar fashion, Chen et al. reported that the HOMO position of CuPc is found to be closer to the E_F than the VBM of $CH_3NH_3PbI_3$. Thereby, it promote hole transfer from $CH_3NH_3PbI_3$ to CuPc.[66] These findings were corroborated from the evolution of core level C1s spectra (Fig. 7d) and the incremental change of BE of the three atomic constituents of CuPc films as a function of molecular thickness (Fig. 7e).

To illustrate the role of substrate, Olthof and Meerholz found that the tuning the energetic alignment of the hybrid perovskite $MAPbI_3$ on four different substrates PEIE, ITO, PEDOT:PSS, and MoO_3 (Figs. 7f-i) were accompanied by the interface dipoles and band bending within the perovskite films.[67] In addition, the work function of the perovskite is influenced by the nature of the substrate that can be manipulated from 4.2 eV for the two low WF substrates, such as PEIE and ITO, to 4.7 eV for the high WF substrates, like PEDOT:PSS and MoO_3. In addition, the work by Miller and coworkers suggested that the insulating and n-type substrates increase the VBM of $MAPbI_3$ toward E_F, indicating the extent of pinning the conduction band to the Fermi level. In the contrary, the p-type substrates decrease the valence band to Fermi energy difference.[50]

Ou and coworkers have employed transition metallic oxide, MoO_3 as a surface dopant to locally tune the charge carrier properties of $CH_3NH_3PbI_3$ perovskite nanosheets as schematically shown in Fig. 7j. A very broad depletion region up span to a few micrometers in the perovskite p-n junction was established based on the complementary detail of SECO (Fig. 7k) and low binding energy region (Fig. 7l). The interface state upon MoO_3 was incrementally introduced to the perovskite in combination with the high work function of MoO_3 led to electron transfer from the perovskite to MoO_3 occurs at the MoO_3/perovskite interface, as schematically depicted in Fig. 7m. For comparison, Arramel et al. used several zethrenes (Fig. 7n) as molecular dopants in which n-type or p-type doping were realized by coating them onto all-inorganic perovskite absorber such as $CsPbBr_3$ (crystal structure is shown in Fig. 7o).[69] The modulation of WF was properly adjusted at the heterointerface such that the efficient electron/hole transfer can be regulated via chemical design as illustrated in Fig. 7p.[70] In summary, several article collections that put an emphasis to tune the interfacial electronic structure on 3D- and 2D-hybrid perovskites is presented in Table **??**.

3. Functionalization of Molecules in Tuning the Optical Properties of Perovskites

Optical properties in 2D perovskite halide materials are important features in determining the characteristics desirable in high performance photovoltaic and optoelectronic devices.[22] For photovoltaics, it is important to highlight the absorption of the materials while for the optoelectronics, we also need to consider the emission wavelengths and lifetimes. In principle, for 2D perovskite halide materials, they are already many reports in photovoltaic applications with the respect of their stability and efficiency,[83–86] while for perovskite light emitting diodes, the attractiveness is the higher quantum efficiencies than those of 3D perovskite halides.[87] Although some optical properties of those 2D perovskite materials are already beyond their siblings of 3D perovskite materials, they are still room of improvements for better devices. In this subchapter, we discuss how the functionalization of molecules can be attractive to enhance the optical characteristics of 2D materials.

3.1. *Tuning the reflection, the transmission, and the absorption*

The important goal for tuning of all these optical properties is to optimize how photovoltaic devices can absorb more lights in such perovskite thin materials. The common methods are by introducing

Table 1.: Summary of organic molecules/hybrid perovskites study

Perovskite	Organic molecules	Techniques	Finding	Ref.
$CH_3NH_3PbI_3$, $CH_3NH_3PbI_{3-x}Cl_x$ and $CH_3NH_3PbBr_3$	Spiro-OMeTAD	UPS and IPES	Band bending of 0.1 eV–0.3 eV in the Spiro-OMeTAD layer.	65
$CH_3NH_3PbI_3$	CuPc	XPS and UPS	0.3 eV band bending was found for the CuPc layer.	66
$CH_3NH_3PbI_3$	C60	UPS and IPES	A high electron-blocking barrier and only a small loss in hole potential energy of 0.2 eV.	23, 71
$CH_3NH_3PbI_3$	PTCDI-C5	XPS and UPS	The electron extraction with a moderate VBM-HOMO offset of ∼0.7 eV.	72
$(FA_{0.83}MA_{0.17})_{0.95}Cs_{0.05}Pb(I_{0.6}Br_{0.4})_3$	Indene-C60 bisadduct (ICBA)	Current density-voltage (J-V)	Passivation by Lewis acid.	73
$FASnI_3$	C60	UPS, IPES, and XPS	Surface treatment with carboxylic acids and bulky ammonium improve the PV performance.	74
$CH_3NH_3PbI_{3-x}Cl_x$	thiophene and pyridine	Current density-voltage (J-V)	Passivation by Lewis bases through coordinate bonding.	75
$CH_3NH_3PbI_3$	L-a-phosphatidylcholine, choline chloride	Current density-voltage (J-V)	Passivation by zwitterions.	76
$CH_3NH_3PbI_{3-x}Cl_x$ and $CH_3NH_3PbI_3$	HATCN and F6TCNNQ	XPS and UPS	Initial perovskite surface state density promote different interface ELA (variations over 0.5 eV)	77
$CH_3NH_3PbI_3$	(Co(C5H5)2)	XPS and photo-conductivity	n-type charge transfer doping by directly depositing the organic small molecule cobaltocene	78
ethylammonium (EA), butylammonium (BA), and phenethylammonium (PEA) of PbI_4	HATCN	Current density-voltage (J-V), electro-luminescence (EL) and PL measurements	organic cation in the 2D perovskite layer plays a critical role in the CT process.	79
EA_2PbI_4 and PEA_2PbI_4	Ethanolamine (EA, $HOCH_2CH_2NH_3^+$)	Photocurrent measurement	the smooth 2D perovskite is less sensitive to ambient moisture and exhibits a considerably low dark current.	
A_2PbI_4	pyrene-$C_4H_8NH_3^+$ and TCNQ or TCNB	Absorption and PL measurements	The incorporation of charge-transfer complexes has a significant influence on the absorption in the visible wavelength region.	

Table 2.: Table **??** (*continued*)

Perovskite	Organic molecules	Techniques	Finding	Ref.
NAP_2PbI_4	TCBQ	Temperature-dependent ultraviolet-visible absorption spectra	Lowering the exciton binding energy relative to the undoped perovskite	[80]
$(C_4H_9NH_3)_2(CH_3NH_3)_3Pb_4I_{13}$ ($(BA)_2(MA)_3Pb_4I_{13}, n = 4$)	Graphene	Current density-voltage (J-V), STM, femtosecond pump-probe spectroscopy.	plane-contacted perovskite and graphene interface presents a lower barrier than gold for charge injection.	[81]
(HEA)-based quasi-2D perovskite materials (n = 9)	halogenated 4-fluorobenzyl-ammonium (FBA) and 4-chloro-benzylammonium (CBA)	UV-Vis absorption, XPS, Current density-voltage (J-V)	0.1CBA-based quasi-2D PSCs achieve a superior PCE of 18.75 %.	[82]
Intended for interface engineering in perovskite solar cell devices				

anti reflection coating[88] or nanostructures[89] on the top of the perovskite photovoltaic films. However, they are currently no report on the anti reflection coating made by functionalization of atomic-thick molecules. Most of the cases, tuning of the absorption is performed through controlling the spacer organic cations through adding molecules in Ruddlesden-Popper phase,[4,85] see Fig. **??**. In this method, we can add more overlaps with the solar spectrum creating more infrared photons to be absorbed by the solar cell.

3.1.1. *Tuning the emission and the energy transfer*

Unlike 3D one, 2D perovskite materials have various profiles in the emission. Figs. 4a and 4b exhibits the photoluminescence (PL) spectra and time-resolved PL (TRPL) decay curves from various perovskite bromides and iodides, respectively while they are related with their structures in Fig. 4c. For perovskite bromides, PL in Fig. 4a, they have narrow and broad emission features. The broad emission spectra shown in (API)$PbBr_4$, (AEIU)$PbBr_4$, and (EDBE)$PbBr_4$ originate from the their (110)-corrugated crystal structures, which is common in early found white light emission perovskites.[90–92] We note that those structures also have very large Stokes shift as large as 1 eV.[93] Such broad emission is related to self-trapped exciton. Another structure with (100)-flat $(CHA)_2PbBr_4$ has two emission bands. Beside that at 520 nm related with self-trapped exciton,[11] it has a narrow band at 425 nm and assigned to the free excitonic emission. $(PEA)_2PbBr_4$ have similar relatively bulky-ring structures as $(CHA)_2PbBr_4$ but it has much more contributions from the narrow band emission. Structures with a linear alkyl chain like $(DAB)_2PbBr_4$, $(BA)_2PbBr_4$, and $(OA)_2PbBr_4$ have the same narrow and broad emission patterns, especially the narrower self-trapped exciton emission in comparison to those of (110)-corrugated and (100)-flat crystal structures.

For perovskite iodides, the emission seems similar with their bromide siblings. In addition, we observe evidence of dual band gap structures, which are characterized by double peaks, in $(BA)_2PbBr_4$ and $(BA)_2PbI_4$ as it was also previously reported in the literature.[94] Decay curves in Fig. 5b were fitted with

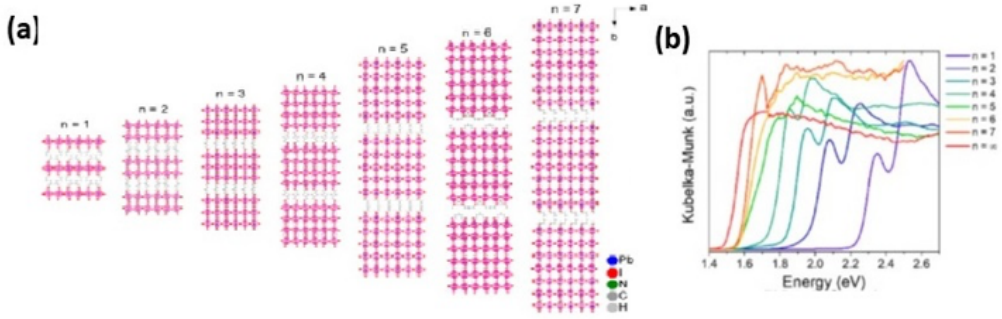

Fig. 4.: (a) Crystal structures and (b) optical absorption spectra of the RP phase $(BA)_2(MA)_{n-1}PbnI_{3n+1}$ (n = 1-7). Figures reproduced from.[4]

Table 3.: Decay components, their averages and their contributions from three-exponential fits of TRPL.

Compounds	Results of fitting	
	Decay components (ns (%))	Average (ns)
(BA)2PbBr4	0.7 (33%), 2.2 (47%), 7.8 (20%)	2.8
(CHA)2PbBr4	1.0 (13%), 2.9 (68%), 9.2 (19%)	3.9
(OA)2PbBr4	0.3 (43%), 0.4 (43%), 2.5 (14%)	0.7
(DAB)PbBr4	0.4 (43%), 0.5 (44%), 4.9 (13%)	1.0
(API)PbBr4	1.5 (26%), 4.0 (59%), 9.6 (15%)	4.2
(AEIU)PbBr4	0.7 (46%), 2.5 (37%), 10.3 (17%)	3.0
(PEA)2PbBr4	2.6 (37%) 6.9 (54%) 19.2 (9%)	6.4
(EDBE)PbBr4	0.3 (2%), 0.4 (2%), 12.9 (96%)	12.4
(BA)2PbI4	0.3 (3%), 0.5 (89%), 1.0 (8%)	0.5
(CHA)2PbI4	0.3 (9%), 1.0 (85%), 9.7 (6%)	1.4
(OA)2PbI4	0.4 (36%), 0.6 (59%), 1.6 (5%)	0.6

three-exponential functions and the average decay times and components are shown in Table **??**.

Most perovskite materials show a fast decay, as fast as 0.6 ns, except $(EDBE)PbBr_4$, whose decay is up to 12.4 n/second. The longer decay for $(EDBE)PbBr_4$ is related to the substantially long lifetime of the exciton self-trapping process which also explains its broad PL spectrum. In addition, the lifetimes of perovskite iodides are much faster in comparison with those of perovskite bromides. The bromides also have brighter emission than iodides under the same excitation power. It seems that fast non-radiative decay processes dominate in the perovskite iodides, causing a quenching in PL and faster decay times.

Adding functionalized molecules in those perovskite materials is useful in terms of tuning the emission spectra. Such method has been shown previously for tuning the absorption via controlling the spacer organic cation.[4,85] Beside tuning the emission, we also expect that through the charge and energy transfers, we also may optimize the emission in to free excitonic path rather than the self-trapped path due to its fast nanosecond emission. However, beside 3D perovskite halide materials,[69,70] there is no report for observation of charge and energy transfers from molecule functionalization of 2D perovskite materials.

Fig. 6 3 shows the example of molecular functionalization of all-inorganic perovskite materials.[69] Previously, we used kinetically-blocked heptazethrene

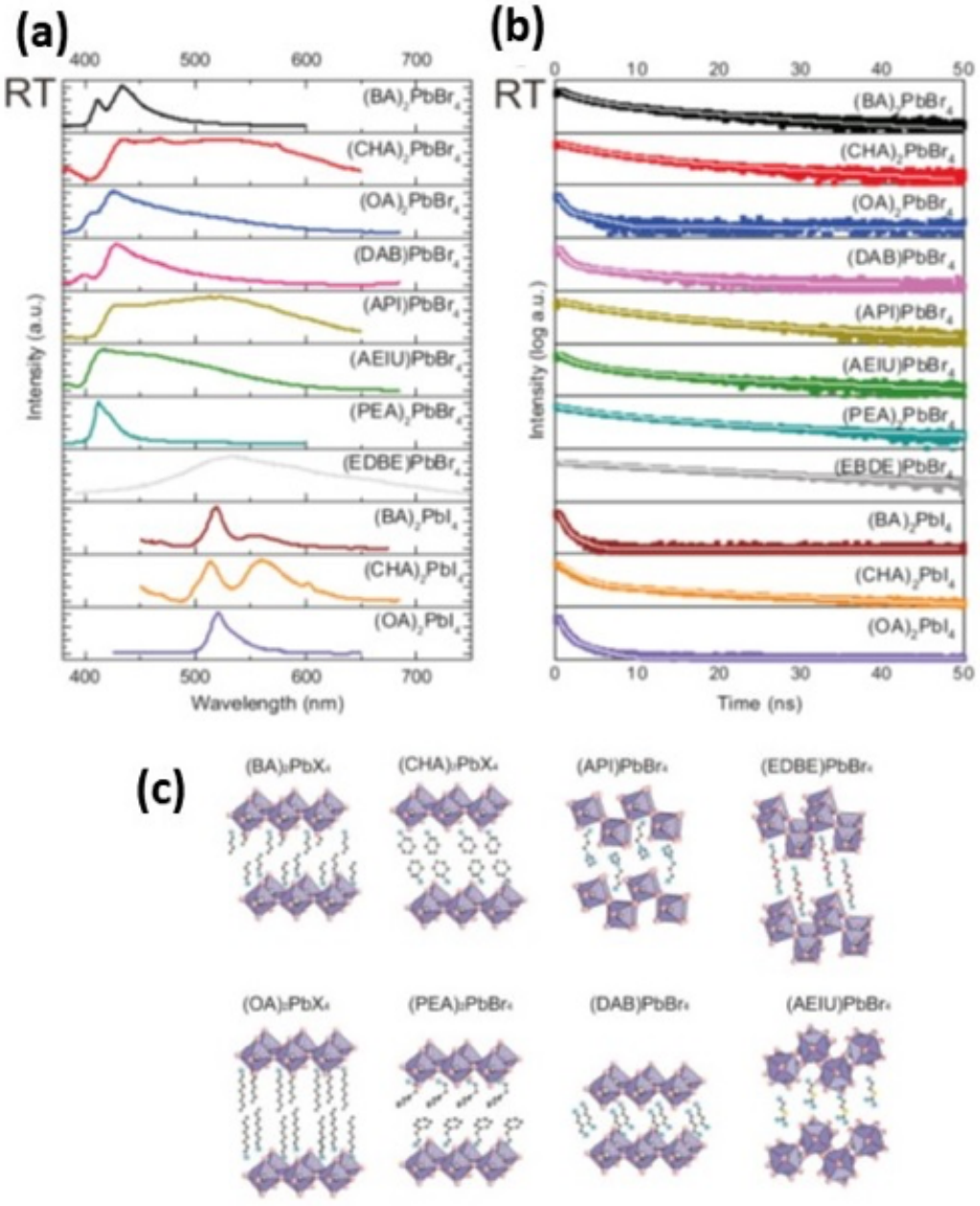

Fig. 5.: (a) Photoluminescence (PL) spectra, (b) time-resolved PL (TRPL) decay curves, and (c) schematic representation structures of the 2D perovskite bromides and iodides. Figures reproduced from.[90]

triisopropylsilyl ethynylene (HZ-TIPS) derivatives and its homologue octazethrene (OZ-TIPS) illustrated in Figs. 6a and 6b as the doping molecules for $CsPbBr_3$ crystals with its structure illustrated in Fig. 6c.

PL spectra of $CsPbBr_3$ crystals before and after doping with HZ-TIPS are presented in Fig. 6d. The HZ-TIPS molecular doping on $CsPbBr_3$ shows three emission peak (424, 446, and 473 nm) that can be associated to the signature of HZ-TIPS. These additional peaks were not observed when we measured the bare perovskite crystal. However, we found that the perovskite PL intensity decreases by 10 folds

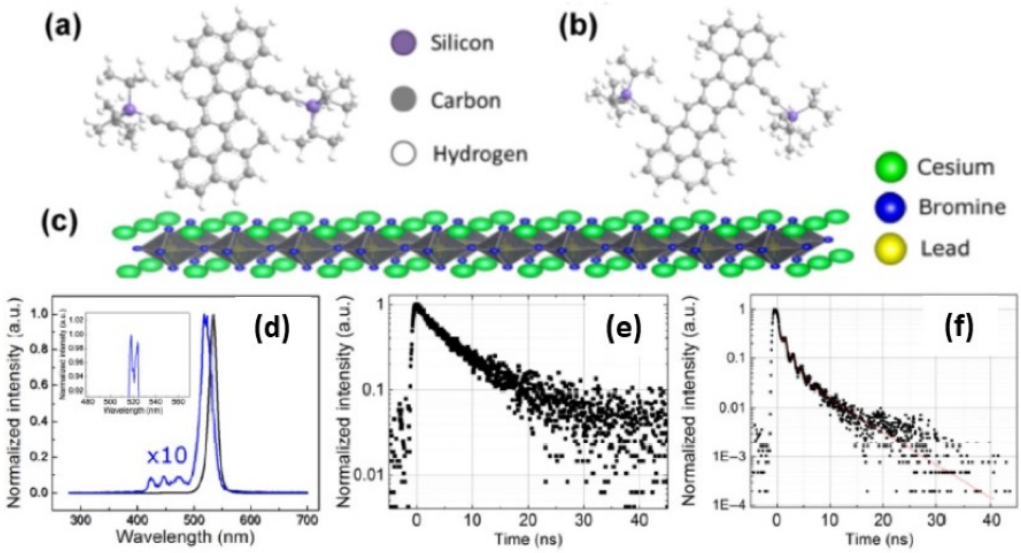

Fig. 6.: (a) and (b) are the ball-stick model structure of HZ-TIPS and OZ-TIPs, respectively. (c) Representation of cubic structure $CsPbBr_3$. (d) PL emission spectra of bare (black solid line) versus HZ-TIPS doped $CsPbBr_3$ (blue solid line). The latter curvature is multiplied by 10 for the sake of guidance for the eye. The inset indicates the enlargement of PL peak that corresponds to the splitting of emission peak. (e) Time-resolved PL decay of bare CsPbBr3 and its corresponding HZ-TIPS doped sample (f). A fitting curve is indicated by the solid red line. Figures reproduced from.[69]

and the excitonic emission of the perovskite emission band is shifted to shorter emission wavelength of about 520 nm with the appearance of two peaks. We attribute the blue shifted emission peak in thermally-deposited HZ-TIPS sample is due to highly efficient charge transfer excited state that provide efficient intramolecular $\pi - \pi$ stacking interactions.[69] For explaining the PL intensity decrease, the TRPL decay curves for both bare and doped crystals are shown in Figs. 6e and 6f, respectively. At a glance, the decay curve from doped crystals yields faster decay times in comparison to that from bare crystals. From the two-exponential fits,[69] the average lifetimes for both bare and doped crystals reported to be 8.3 and 3.6 ns, respectively. The emission in doped crystal is much faster by 2.3 times than that of bare crystal showing a consistent PL quenching after addition of HZ-TIPS molecules. In the same paper,[69] we also noticed that the OZ-TIPS molecule functionalization is responsible for the decrease of the emission intensity and the lifetime by factors of 12 and 2.9 times, respectively. Using data from XPS, UPS, and NEXAFS measurements, we later conclude that this quenching is related to the charge transfer event at the interface and this may affect the excitonic emission at the interface.[69,70] However, those studies are still in the infancy level so that further investigations are needed to improve so that we can suppress the non radiative recombination in the molecular functionalization while at the same time, we can optimize the charge transfer for the fast radiation recombination route. Such faster emission properties will be useful for modulation of the light emitting diodes for light fidelity in the communication technology.[95]

4. Applications

Perovskite materials have excellent optoelectronic properties for the applications of solar cells[96] and light emitting devices.[97] In this section, the applications of particularly 2D perovskites are discussed in solar cells for enhancing light absorption and improving photo-generated carrier extraction for solar cells, and in light-emitting diode for improving extraction efficiencies and tuning the color.

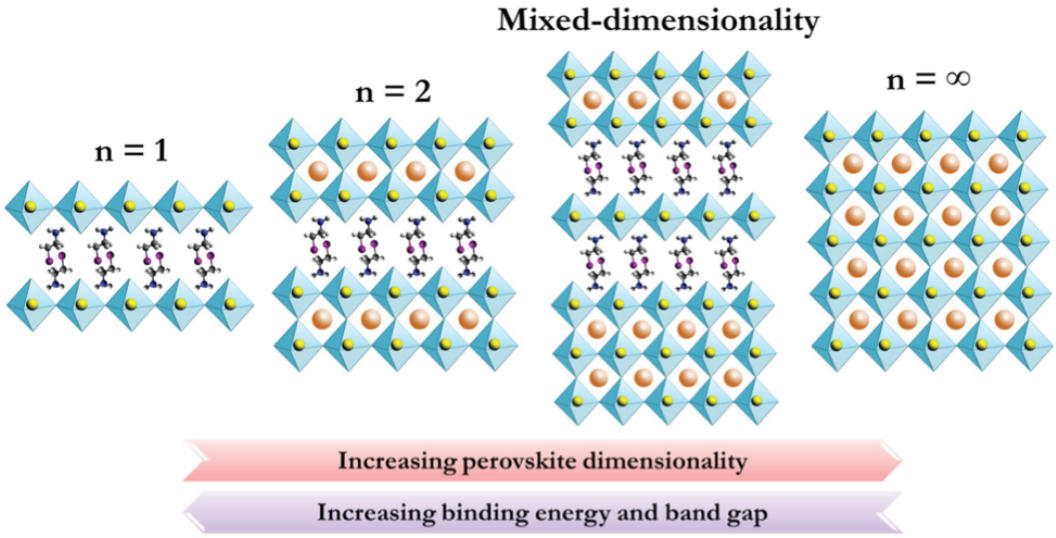

Fig. 7.: Illustration of crystalline structure of 2D perovskites ($n = 1$ and 2, where n represents the metal halide lattices), mixed dimensionality perovskites and 3D perovskites ($n = \infty$).[98]

4.1. *Enhancing Light Absorption in Photovoltaic Cells*

In the past decade, perovskite materials particularly for organic-inorganic halides have attracted many interests in photovoltaic application due to the excellent optical and electrical properties.[99] As reducing the perovskite dimension from 3D to 2D, unique properties appear due to quantum confinement effect[100,101] and the enhancement of stability offers new approaches to stabilizing perovskite-based photovoltaic devices.[12,85] Fig. 7 illustrates the crystalline structure of 2D perovskites, mixed dimensionality and 3D perovskites.[98] In 2D perovskites, the optoelectronic properties are greatly impacted by its tunable structure of organic layers based on the used spacer cations such as alkyl chain length, insertion of π-conjugated segment to facilitate charge transport, and ammonium dications, while its superior air stability is improved by the hydrophobic nature of organic spacer and the van der Waals force interactions between the adjacent layers.[102] The first generation of solar cells based on $PEA_2MA_2Pb_3I_{10}$ ($PEA{:}C_6H_5(CH_2)_2NH_3^+$, MA: $CH_3NH_3^+$) with a planar device configuration was reported to be more resistant to moisture and be able to be fabricated under humid conditions, although the exhibited PCE of 4.73 % was lower compared to that of $MAPbI_3$ based solar cells.[103] Later, 2D $BA_2MA_{n-1}Pb_nI_{3n+1}$ ($BA{:}CH_3(CH_2)_3NH_3^+$, $n = 1, 2, 3$, and 4) perovskite thin films was reported to have decreasing the band gaps of the series with increasing n values, from 2.24 eV for $n = 1$ to 1.60 eV for $n = 4$, and finally 1.52 eV for $n = \infty$ ($MAPbI_3$), while the films displayed an ultrahigh coverage due to the orientation of $[Pb_3I_{n+1}]^-$ perpendicular to the substrate surface with the maximum PCE of 4.02 % featuring Voc of 929 mV and Isc of 9.42 mA cm^{-2} for $BA_2MA_2Pb_3I_{10}$ ($n = 3$) remained its performance after long exposure to a high-humidity environment.[86] To overcome the inhibition of out-of-plane charge transport by organic cations acting like insulating layer between the conducting inorganic slabs, near-single-crystalline quality $BA_2MA_3Pb_4I_{13}$ layered perovskite was grown through hot-casting technique with a strongly preferential out-of-plane alignment with respect to the contacts in the planar solar cells to facilitate the efficient charge transport and as consequently PCE could reach up to 12.52 % without hysteresis.[12] In comparison to films casted at room temperature, the hot casted 2D perovskite films showed the enhanced crystal quality of substantially larger grains (400 nm) and much lower pinholes, and additionally the lack of Urbach tails in the optical absorption, the very small Stokes shift, and the strong absorption and photoluminescence indicating that the films behaved like a direct-band gap intrinsic semiconductor with the excellent crystallinity, low trap concentration and

little disorder-induced density of states in the band gap.[12] Using the short branched chain spacer cations (iso-BA^+) compared to conventional linear n-BA^+ has showed the remarkable increase in the optical absorption and crystallinity.[100] In fact, the performance of 2D perovskite still lags behind 3D counterpart, particularly with the low open circuit voltage indicating the presence of non-radiative recombination process caused by inhomogeneous energy landscape which introduces extra energy loss, creates band tail states and inhibits minority carrier transport.[104] By using (aminomethyl) piperidinium quasi-two-dimensional (quasi-2D) perovskites and controlling carefully their crystallization kinetics, the lowest energy distribution and homogeneous energy landscape could be achieved with the significant reduction of the Shockley-Read-Hall recombination and suppression of the quasi-Fermi level splitting, resulting in excellent PCE of 16.53 % and Voc of 1.21 V.[104] For further enhancement of optical absorption, tandem solar cell architecture offers the opportunity to match the spectral distribution of solar light, in which the wider band gap of semiconductor is suitable as higher bandgap absorber and vice versa. A mixed Sn-Pb narrow-bandgap perovskite anchored with ultrathin 2D layer for defect passivation at the interface and grain boundaries, and the combination of this passivated narrow band gap with a wide-bandgap perovskite in two terminal tandem solar cells, could achieved the stabilized PCE of 23.5 %.[105] Moreover, the employment of wide-bandgap perovskite passivated with 2D/3D perovskite heterostructure in four terminal tandem configurations i.e. perovskite/c-Si and perovskite/CIGS solar cells showed the stabilized PCEs of up to 25.7 % and 25.0 %, respectively.[106] Further utilization of 2D/3D perovskite heterostructure for better solar cells is also described in the next section.

4.2. *Improving Photo-generated Carrier Extraction in Photovoltaic Cells*

Interfacing 2D perovskites with an organic semiconductor has been found to form donor/acceptor charge transfer states at this heterojunction, which dissociates excitons in 2D perovskites and thus increases the photocurrent production with the organic cation size in the 2D perovskite layer playing a critical role in this charge transfer process.[79] For efficient solar cells, the presence of long-lived charge carriers is needed so that the charges can be extracted before significant recombination occurs, in which the diffusion length should be longer than the required thickness for complete light absorption.[109] To enhance the charge transport, using small propane-1,3-diammonium (PDA) cation in 2D perovskite could reduce the interlayer distance in 2D perovskite and thus yield the PCE of 13 %.[110] Recently, in-plane carrier diffusion length in 2D $(BA)_2PbI_4$ perovskite has been determined to be 1.82 µm.[111] Furthermore, doping 2D $BA_2MA_3Pb_4I_{13}$ perovskite with Cs by replacing MA^+ with Cs^+ has been proposed to improve the optoelectronic properties in terms of trap density, charge-carrier mobility, and charge-transfer kinetics, in which the PCE could increase from 12.3 % to 13.7 % in comparison to un-doped perovskite.[83] Controlling the crystallization kinetics by appropriate partial substitution of MA cation with formamidinium ($NH_2CH{=}NH_2^+$ or FA) cation in $BA_2MA_3Pb_4I_{13}$ perovskite could increase the grain size and limit the non-orientated phase, leading to reduced non-radiative recombination centers.[112] Furthermore, interfaces also dominate the charge-charge recombination and initiate the degradation process, thus affecting the photovoltaic performance. Thus modification on perovskite layer surface is promising to reduce the interfacial recombination and improve the stability. Controlling the electron density distribution of passivation molecules with a donor-π-acceptor structure has been approached as a strategy to optimize the defect passivation in the perovskite solar cells.[113] Phenethylammonium iodide (PEAI) treatment of methylammonium lead iodide ($MAPbI_3$) perovskite reduces the surface defects and suppress the non-radiative recombination resulting in higher photovoltaic performances with 23.32 % efficiency achieved.[114] On the contrary, PEAI treatment at the $MAPbI_3$/C60 interface showed the decrease in electron affinity and ionization energy, thus hindering electron transfer from $MAPbI_3$ to C60 and decreasing the performance consequently.[115] This surface energetic change upon ligand application indicates that an appropriate selection of surface ligand is necessary for favorable energy alignment based on

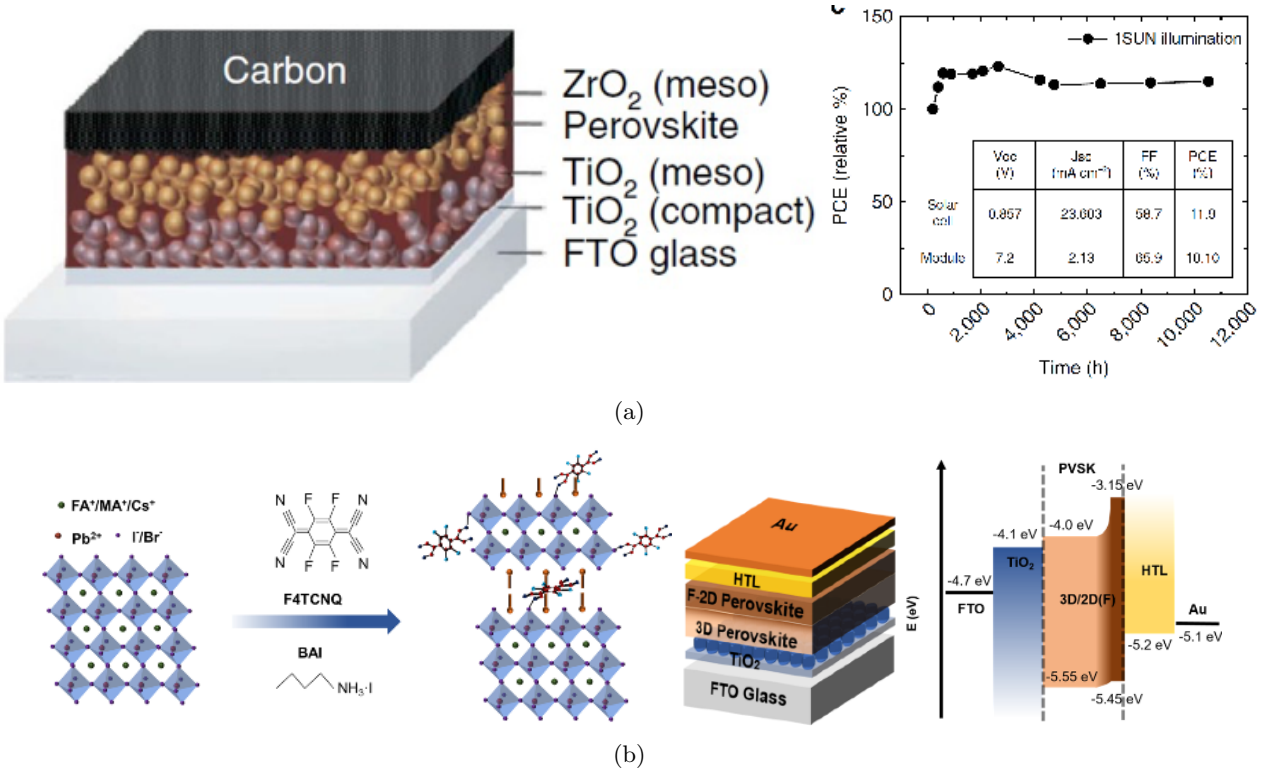

Fig. 8.: (a) Module stability test of 2D/3D perovskite with 3 % AVAI in HTM-free solar cell and in HTM-free 10×10 cm^2 module under 1 sun AM 1.5 G conditions at stabilized temperature of 550 °C and at short circuit conditions.[107] (b) Schematics of 3D/2D/F4TCNQ perovskite deposition (left), solar cell device architecture (middle) and corresponding energy level landscape (right).[108]

where the treatment will be carried out either at perovskite/electron transfer layer or perovskite/hole transfer layer interface.[115] At the interface between $FASnI_3$ (FA: formamidinium) and C60, favorable energy landscape for electron transfer from $FASnI_3$ to C60 has been reported with and without the surface ligand, likely due to iodide diffusion out of $FASnI_3$ into C60 resulting in n-doping of C60, while surface ligand would greatly improve the stability of $FASnI_3$ solar cells.[74] In interface engineering, doped charge-transporting layers in planar perovskite solar cells have been regarded as an efficient pathway to enhance photovoltaic performances.[116] In addition to surface ligand, 2D perovskites have been also considered as passivating materials in improving the performance and stability of lead halide perovskite solar cells. By interface engineering an ultrastable 2D/3D $(HOOC(CH_2)_4NH_3)_2PbI_4/MAPbI_3$ perovskite junction, one-year stable perovskite devices could be achieved, opening the way for the realization of highly efficient and stable perovskite solar cells for widespread practical deployment, shown in Fig. 8a.[107] By spin-coating a phenylformamidinium iodide (PFAI) solution on the formamidinium (FA)-based perovskite film surface of $Cs_{0.05}Rb_{0.05}(FA_{0.83}MA_{0.17})Pb(I_{0.95}Br_{0.05})_3$, the perovskite surface defects and the recombination at the interface between the perovskite layer and the hole transport layer are reduced by the mixed-cation 2D perovskite acting as surface "patches", thus resulting in the improved photovoltaic performance and stability.[117] Mixed 2D/3D hybrid perovskite system offers a promising pathway to obtain chemical/photochemical stability compared to 3D counterpart while gathering the significant properties of 3D in terms of band gap tuning through number of layers.[118] As shown in Fig. 8b, further introduction of molecule additive (i.e. 2,3,5,6-tetrafluoro-7,7,8,8-tetracyanoquinodimethane or F4TCNQ) into the 2D layer in 3D/2D perovskite solar cells, improved charge extraction and reduced charge recombination

with the maximum PCE of 20.2 % compared with 18.2 % for unmodified 2D capping layers.[108] Here, the strong electron-acceptor characteristic of F4TCNQ enables it to undergo partial charge transfer with the perovskite layer to provide a passivation effect, which also modifies the crystalline domain sizes of the 2D perovskite. 2D/3D perovskite heterostructure on top of the 3D $MA_{1-y}FA_yPbI_{3-x}Cl_x$ perovskite with modulated diffusion passivation by introducing PEAI and N,N-dimethylformamide (DMF) as an additive could achieved a high PCE of up to 22.18 % due to a significant increase of Voc and FF.[119] Along with these material and device development, advanced characterization tools have also become necessary to provide further understanding and to overcome the existing challenges on the road to commercialization.[120]

4.3. *Improving Extraction Efficiencies in light emitting diode (LED)*

Due to the material properties of perovskite as well as low-cost fabrication and solution processability, many groups have shown a great deal of attention towards the development of perovskite light emitting diodes (PeLEDs) and research activities are rapidly increasing.[?] Particularly, 2D perovskites have exciton binding energies of about 300 meV. Not only greater than those of 3D perovskites, the amount is also an advantage in the field of optoelectronics.[?]

Halide perovskite (HP) platelets possess good optical and electrical properties suitable for LED applications. Yet due to the challenge in producing a uniform film, only a small number of reports recorded their role as LED materials. Ling et al. used $MAPbBr_3$ nanoplatelets to create green LEDs.[?] The 2D $FAPbBr_3$ dielectric quantum well was investigated by Kumar et al., who managed to improve the photoluminescence quantum yield (PLQY) up to 92 %.[?] The same material also yielded LEDs with a maximum current efficiency of 13.02 cd A^{-1} and external quantum efficiency (EQE) of 3.04 %.[?] A success in creating blue LEDs has also been reported. Yang et al. made blue LEDs with sharp emission at 480 nm by controlling the thickness of $CsPbBr_3$ with high precision at the atomic scale.[?]

One way to improve the LED's performance is through multi-dimensional HPs. By adding more layers and creating a quasi-2D perovskites, the EQE can be improved. The multiple quantum wells in the quasi-2D perovskites facilitate exciton formation and lower the possibility of exciton dissociation. The EQEs of quasi-2D PeLEDs have achieved around 10 % and highest EQEs of 11.7 % in near-infrared region was obtained.[121,122]

Knowing that the perovskite could be a good candidate for an emitting material, the overall emission can be further improved by surface passivation. The effect of trioctylphosphine oxide (TOPO) deposition, spin-coated onto the perovskite layer, has been proven able to significantly increase the PLQY of an $n = 3$ composition of $PEA_2(FAPbBr_2)_{n-1}PbBr_4$ perovskite from 57.3 % to 73.8 %. The average fluorescence lifetime of the $n = 3$ composition film is also increased from 0.17 µs to 0.36 µs after TOPO treatment.[123] Fig. 9 shows the band alignment and the cross-section of a PeLED structure where the perovskite layer is glstopo coated as well as the electroluminescence characteristics of the resulting device.

Electron transport layers (ETLs) and HTLs are utilized in photovoltaic cells to optimize the charge carrier injection and blocking functions. Similarly in PeLEDs, the improvements in EQE can be made through better choice and quality of the ETL and HTL.[124]

4.4. *Tuning Color in LED*

PeLEDs have attracted intense research interest due to their remarkable properties, including a tunable bandgap, high PLQY, and high color purity. Although green- and near-infrared-emitting PeLEDs have recently arrived at an impressive level of EQEs,[?] fabricating efficient and color-stable blue PeLEDs useful for lighting and displays still requires further extensive study.

The bandgap plays a big role in determining the emission wavelength of a LED. In a conventional three dimensional perovskite structure, it can easily be tuned monotonically by adjusting the halogen component. The emission wavelength between

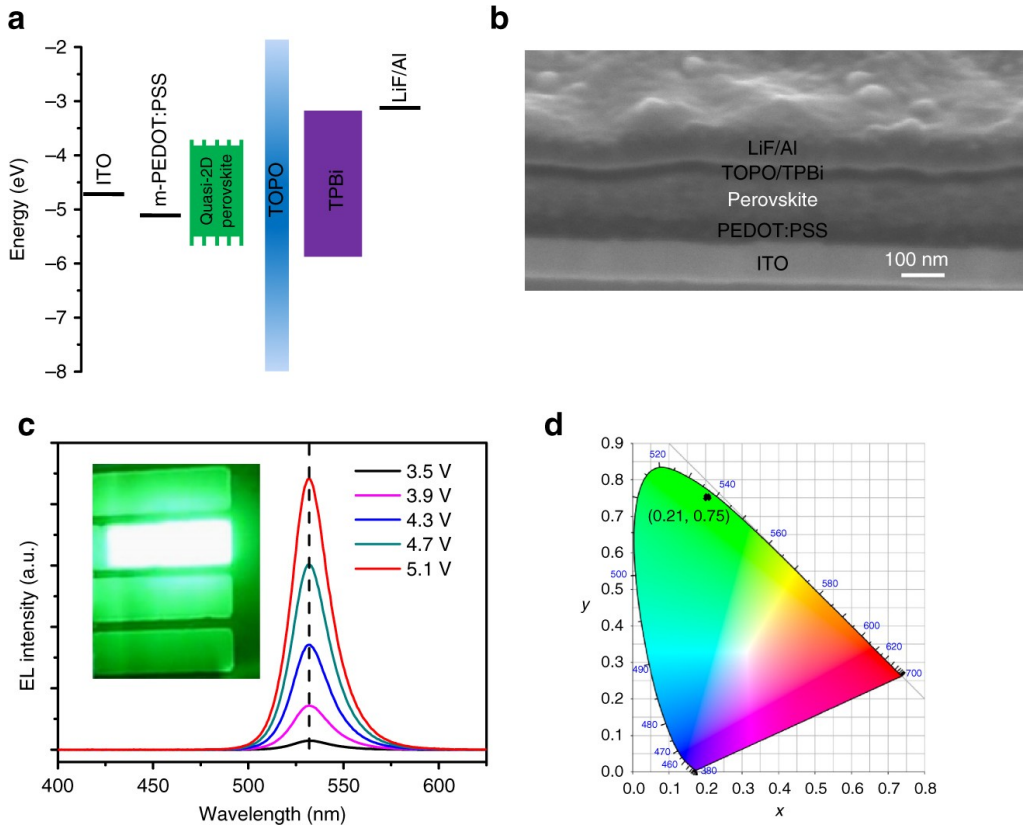

Fig. 9.: Perovskite light-emitting diodes structure and electroluminescence. (a) Band alignment of each function layer in the devices. (b) Cross-section scanning electron microscopy (SEM) image of the device, the scale bar is 100 nm. (c) Typical electroluminescence (EL) spectra of $PEA_2(FAPbBr_3)_{n-1}PbBr_4$ ($n = 3$ composition) based PeLEDs under different voltage bias. Inset shows the electroluminescence image of PeLEDs. (d) The corresponding Commission Internationale de l'Eclairage (CIE) coordinate of typical PeLEDs based on $PEA_2(FAPbBr_3)_{n-1}PbBr_4$ ($n = 3$ composition).[123]

450 nm and 490 nm can be achieved through incorporating Cl:Br-mixed halide perovskites as the emissive material. Unfortunately, illumination and voltage bias both lead to a side effect, namely undesirable shifts in electroluminescence (EL) wavelength from blue to green during device operation.[124,125]

Quasi-2D perovskites follow a different procedure to deliver blue PeLEDs. They are smaller in terms of structure dimension and possess a long-chain ligand such as butylammonium (BA) or phenyletylammonium (PEA) as B in the standard formula of $B_2A_{n-1}M_nX_{3n+1}$. Since quasi-2D perovskites consist of a finite amount of inorganic layers (n), we can tune their bandgap simply through reducing the number of total layers. Quan et al. recorded the tuning of bandgap in quasi-2D perovskites from ca. 2.6 eV ($n = 4$), to 2.7 eV ($n = 3$), 2.9 eV ($n = 2$), and 3.1 eV ($n = 1$).[126] Still, reported quasi-2D blue PeLEDs exhibit poor color stability under LEDs operation.[127–131] The low stability originated from multiple emission peaks from mixed phases, leading to inefficient charge transfer and various emission features conditional to bias voltage. To balance out the different phases, hoping to achieve even crystallization, long ligands PEA are substituted by shorter ones (isopropylammonium (IPA)).[124]

The maximum luminescence and the maximum EQE were measured from varying devices. Luminance (L) is proportional to the product of current density (J) and efficiency (EQE), signalling that luminance is affected by both current density and efficiency. Although thinner films lead to higher J,

their EQE are not always higher. The perovskite thickness reduction would result in a higher chance of charge carrier leakage and hence produce lower EQE.

Apart from experimenting with the emissive layer, the selection of HTL material can also contribute to the peak wavelength of the PeLED. Recent study suggests that NiO_x, PVK, and PEDOT:PSS help provide better emission color stability during device operation.[124]

Not only do 2D perovskites have excitonic emission, they also possess an intriguing optical property, which is the broadband emission. This type of emission is triggered by the rich chemical tunability in 2D metal halide perovskites. If the emission covers the entire visible spectrum, the emitters can act as single-source white-light emitters superior to current mixed phosphor based technology in terms of energy-efficiency. The 2D perovskite based single-source white-light emitters and their development belong to the emerging research field. Since the work from Karunadasa et al. in 2014,[?] which demonstrated bright broadband visible emission in 2D perovskite (EDBE)PbX_4 and (N-MEDA)$PbBr_{4-x}Cl_x$, (N-MEDA: N^1-methylethane-1,2-diammonium; EDBE: 2,2-(ethylenedioxy)bis(ethylammonium); X: Cl, Br), several other compositions have been investigated for broadband emission. Some research groups are convinced that the broadband emission is due to crystal defects, but in general, it is believed that the exciton self-trapping phenomenon is behind the broadband emission mechanism. Chen et al. recently proved that introducing impurity through Sn doping in PEA_2PbI_4 can provoke extrinsic self-trapping, yielding broadband red-to-near-infrared emission at room temperature. This as well as a similar observation by Mitzi et al. on modification of the optical and electrical properties using metal impurities, led to a novel strategy in the development of broadband-emitting—that is, dopant-induced extrinsic exciton self-trapping approach.[?]

5. Summary

Recent efforts to negate the effect of unintentional defects that reside within the hybrid perovskites structure has led the community to implement diverse candidates of organic molecules as passivating agents. While 2D-HOIPs intrinsically has a promising solution to overcome the perturbation from the light and moisture instabilities, these emergent materials are mostly suffers ionic migration that pinpointed to the internal defects at the vicinity of topmost perovskite surface or within the inorganic sheets. In this review, we have highlighted several examples to avoid large energy offset, which is feasible by selecting suitable hole/electron transport materials in solar cell devices. In addition, the current knowledge to combat a structural deformation within 2D-HOIPs that alter the perovskite surface is underway by depositing organic adlayers with different molecular functionalization. Here, we also conceptually revisit several important knowledge such as interfacial dipole, band bending and charge transfer that requires careful interpretation for understanding the 2D-HOIPs/organic molecules heterointerfaces.

References

1. D. B. Mitzi, *J. Chem. Soc., Dalton Trans.* (2001) 1.
2. D. B. Mitzi, *Hybrid Organic-Inorganic Electronics* (John Wiley & Sons, Ltd, 2003), ch. 10, pp. 347–386.
3. C. C. Stoumpos, D. H. Cao, D. J. Clark, J. Young, J. M. Rondinelli, J. I. Jang, J. T. Hupp and M. G. Kanatzidis, *Chemistry of Materials* **28** (2016) 2852.
4. L. Mao, C. C. Stoumpos and M. G. Kanatzidis, *Journal of the American Chemical Society* .
5. D. B. Straus and C. R. Kagan, *The Journal of Physical Chemistry Letters* **9** (2018) 1434.
6. C. Ortiz-Cervantes, P. Carmona-Monroy and D. Solis-Ibarra, *Chem. Sus. Chem.* **12** (2019) 1560.
7. C. Katan, N. Mercier and J. Even, *Chemical Reviews* **119** (2019) 3140.
8. Y. Gao, Z. Wei, S.-N. Hsu, B. W. Boudouris and L. Dou, *Mater. Chem. Front.* **4** (2020) 3400.
9. T. A. Berhe, W.-N. Su, C.-H. Chen, C.-J. Pan, J.-H. Cheng, H.-M. Chen, M.-C. Tsai, L.-Y. Chen, A. A. Dubale and B.-J. Hwang, *Energy Environ. Sci.* **9** (2016) 323.
10. A. Oranskaia, J. Yin, O. M. Bakr, J.-L. Brédas and O. F. Mohammed, *The Journal of Physical Chemistry Letters* **9** (2018) 5474.
11. M. D. Smith, B. A. Connor and H. I. Karunadasa, *Chemical Reviews* **119** (2019) 3104.
12. H. Tsai, W. Nie, J.-C. Blancon, C. C. Stoumpos, R. Asadpour, B. Harutyunyan, A. J. Neukirch, R. Verduzco, J. J. Crochet, S. Tretiak, L. Pedesseau, J. Even, M. A. Alam, G. Gupta, J. Lou, P. M. Ajayan, M. J. Bedzyk, M. G. Kanatzidis and A. D. Mohite, *Nature* **536** (2016) 312.

13. C. C. Stoumpos, C. M. M. Soe, H. Tsai, W. Nie, J.-C. Blancon, D. H. Cao, F. Liu, B. Traoré, C. Katan, J. Even, A. D. Mohite and M. G. Kanatzidis, *Chem* **2** (2017) 427.
14. T. Ishihara, J. Takahashi and T. Goto, *Solid State Communications* **69** (1989) 933 .
15. X. Hong, T. Ishihara and A. V. Nurmikko, *Phys. Rev. B* **45** (1992) 6961.
16. L. Dou, A. B. Wong, Y. Yu, M. Lai, N. Kornienko, S. W. Eaton, A. Fu, C. G. Bischak, J. Ma, T. Ding, N. S. Ginsberg, L.-W. Wang, A. P. Alivisatos and P. Yang, *Science* **349** (2015) 1518.
17. B. Saparov and D. B. Mitzi, *Chemical Reviews* **116** (2016) 4558.
18. S. Zhao, C. Lan, H. Li, C. Zhang and T. Ma, *The Journal of Physical Chemistry C* **124** (2020) 1788.
19. L. Mao, W. Ke, L. Pedesseau, Y. Wu, C. Katan, J. Even, M. R. Wasielewski, C. C. Stoumpos and M. G. Kanatzidis, *Journal of the American Chemical Society* **140** (2018) 3775.
20. X. Li, W. Ke, B. Traoré, P. Guo, I. Hadar, M. Kepenekian, J. Even, C. Katan, C. C. Stoumpos, R. D. Schaller and M. G. Kanatzidis, *Journal of the American Chemical Society* **141** (2019) 12880.
21. X. Tian, Y. Zhang, R. Zheng, D. Wei and J. Liu, *Sustainable Energy Fuels* **4** (2020) 2087.
22. F. Zhang, H. Lu, J. Tong, J. J. Berry, M. C. Beard and K. Zhu, *Energy Environ. Sci.* **13** (2020) 1154.
23. T. Hellmann, C. Das, T. Abzieher, J. A. Schwenzer, M. Wussler, R. Dachauer, U. W. Paetzold, W. Jaegermann and T. Mayer, *Advanced Energy Materials* **10** (2020) 2002129.
24. C. M. Mauck and W. A. Tisdale, *Trends in Chemistry* **1** (2019) 380.
25. N. Marinova, S. Valero and J. L. Delgado, *Journal of Colloid and Interface Science* **488** (2017) 373 .
26. Z.-K. Tan, R. S. Moghaddam, M. L. Lai, P. Docampo, R. Higler, F. Deschler, M. Price, A. Sadhanala, L. M. Pazos, D. Credgington, F. Hanusch, T. Bein, H. J. Snaith and R. H. Friend, *Nature Nanotechnology* **9** (2014) 687.
27. H. Jin, E. Debroye, M. Keshavarz, I. G. Scheblykin, M. B. J. Roeffaers, J. Hofkens and J. A. Steele, *Mater. Horiz.* **7** (2020) 397.
28. S. Béchu, M. Ralaiarisoa, A. Etcheberry and P. Schulz, *Advanced Energy Materials* **n/a** (2020) 1904007.
29. W.-J. Yin, T. Shi and Y. Yan, *Advanced Materials* **26** (2014) 4653.
30. K. X. Steirer, P. Schulz, G. Teeter, V. Stevanovic, M. Yang, K. Zhu and J. J. Berry, *ACS Energy Letters* **1** (2016) 360.
31. A. Walsh, D. O. Scanlon, S. Chen, X. G. Gong and S.-H. Wei, *Angewandte Chemie International Edition* **54** (2015) 1791.
32. C. Eames, J. M. Frost, P. R. F. Barnes, B. C. O'Regan, A. Walsh and M. S. Islam, *Nature Communications* **6** (2015) 7497.
33. Z. Ni, C. Bao, Y. Liu, Q. Jiang, W.-Q. Wu, S. Chen, X. Dai, B. Chen, B. Hartweg, Z. Yu, Z. Holman and J. Huang, *Science* **367** (2020) 1352.
34. K. Gauthron, J.-S. Lauret, L. Doyennette, G. Lanty, A. A. Choueiry, S. Zhang, A. Brehier, L. Largeau, O. Mauguin, J. Bloch and E. Deleporte, *Opt. Express* **18** (2010) 5912.
35. W. K. Chong, K. Thirumal, D. Giovanni, T. W. Goh, X. Liu, N. Mathews, S. Mhaisalkar and T. C. Sum, *Phys. Chem. Chem. Phys.* **18** (2016) 14701.
36. N. Liu, P. Liu, H. Zhou, Y. Bai and Q. Chen, *The Journal of Physical Chemistry Letters* **11** (2020) 3521.
37. D. Ghosh, D. Acharya, L. Pedesseau, C. Katan, J. Even, S. Tretiak and A. J. Neukirch, *J. Mater. Chem. A* **8** (2020) 22009.
38. J. Hieulle, C. Stecker, R. Ohmann, L. K. Ono and Y. Qi, *Small Methods* **2** (2018) 1700295.
39. S. Sahare, P. Ghoderao, S. B. Khan, Y. Chan and S.-L. Lee, *Nanoscale* **12** (2020) 15970.
40. M. Telychko and J. Lu, *Nano Materials Science* **1** (2019) 260.
41. B. Chen, P. N. Rudd, S. Yang, Y. Yuan and J. Huang, *Chem. Soc. Rev.* **48** (2019) 3842.
42. J. Xue, R. Wang and Y. Yang, *Nature Reviews Materials* **5** (2020) 809.
43. L. K. Ono, S. F. Liu and Y. Qi, *Angewandte Chemie International Edition* **59** (2020) 6676.
44. J. Chen and N.-G. Park, *ACS Energy Letters* **5** (2020) 2742.
45. H. Hertz, *Annalen der Physik* **267** (1887) 983.
46. A. Einstein, *Annalen der Physik* **322** (1905) 891.
47. *Electron Spectroscopy* (John Wiley Sons, Ltd, 2019), ch. 1, pp. 1–18.
48. R. L. Z. Hoye, P. Schulz, L. T. Schelhas, A. M. Holder, K. H. Stone, J. D. Perkins, D. Vigil-Fowler, S. Siol, D. O. Scanlon, A. Zakutayev, A. Walsh, I. C. Smith, B. C. Melot, R. C. Kurchin, Y. Wang, J. Shi, F. C. Marques, J. J. Berry, W. Tumas, S. Lany, V. Stevanović, M. F. Toney and T. Buonassisi, *Chemistry of Materials* **29** (2017) 1964.
49. B. Philippe, B.-W. Park, R. Lindblad, J. Oscarsson, S. Ahmadi, E. M. J. Johansson and H. Rensmo, *Chemistry of Materials* **27** (2015) 1720.
50. E. M. Miller, Y. Zhao, C. C. Mercado, S. K. Saha, J. M. Luther, K. Zhu, V. Stevanović, C. L. Perkins and J. van de Lagemaat, *Phys. Chem. Chem. Phys.* **16** (2014) 22122.
51. P. Schulz, D. Cahen and A. Kahn, *Chemical Reviews* .
52. J. Emara, T. Schnier, N. Pourdavoud, T. Riedl, K. Meerholz and S. Olthof, *Advanced Materials* **28** (2016) 553.

53. X. Wu, M. T. Trinh, D. Niesner, H. Zhu, Z. Norman, J. S. Owen, O. Yaffe, B. J. Kudisch and X. Y. Zhu, *Journal of the American Chemical Society* **137** (2015) 2089.
54. M. Kollár, L. Ćirić, J. H. Dil, A. Weber, S. Muff, H. M. Ronnow, B. Náfrádi, B. P. Monnier, J. S. Luterbacher, L. Forró and E. Horváth, *Scientific Reports* **7** (2017) 695.
55. F. Zhang, S. H. Silver, N. K. Noel, F. Ullrich, B. P. Rand and A. Kahn, *Advanced Energy Materials* **10** (2020) 1903252.
56. S. Silver, Q. Dai, H. Li, J.-L. Brédas and A. Kahn, *Advanced Energy Materials* **9** (2019) 1901005.
57. Q.-K. Wang, R.-B. Wang, P.-F. Shen, C. Li, Y.-Q. Li, L.-J. Liu, S. Duhm and J.-X. Tang, *Advanced Materials Interfaces* **2** (2015) 1400528.
58. T. C. Sum, S. Chen, G. Xing, X. Liu and B. Wu, *Nanotechnology* **26** (2015) 342001.
59. J.-M. Yang, Y. Luo, Q. Bao, Y.-Q. Li and J.-X. Tang, *Advanced Materials Interfaces* **6** (2019) 1801351.
60. L. Qiu, S. He, L. K. Ono and Y. Qi, *Advanced Energy Materials* **10** (2020) 1902726.
61. S. Shao and M. A. Loi, *Advanced Materials Interfaces* **7** (2020) 1901469.
62. L. K. Ono and Y. Qi, *The Journal of Physical Chemistry Letters* **7** (2016) 4764.
63. S. Wang, T. Sakurai, W. Wen and Y. Qi, *Advanced Materials Interfaces* **5** (2018) 1800260.
64. W. Tress, K. Leo and M. Riede, *Advanced Functional Materials* **21** (2011) 2140.
65. P. Schulz, E. Edri, S. Kirmayer, G. Hodes, D. Cahen and A. Kahn, *Ener. Env. Sci.* **7** (2014) 1377.
66. S. Chen, T. W. Goh, D. Sabba, J. Chua, N. Mathews, C. H. A. Huan and T. C. Sum, *APL Materials* **2** (2014) 081512.
67. S. Olthof and K. Meerholz, *Scientific Reports* **7** (2017) 40267.
68. Q. Ou, Y. Zhang, Z. Wang, J. A. Yuwono, R. Wang, Z. Dai, W. Li, C. Zheng, Z.-Q. Xu, X. Qi, S. Duhm, N. V. Medhekar, H. Zhang and Q. Bao, *Advanced Materials* **30** (2018) 1705792.
69. Arramel, H. Pan, A. Xie, S. Hou, X. Yin, C. S. Tang, N. T. Hoa, M. D. Birowosuto, H. Wang, C. Dang, A. Rusydi, A. T. S. Wee and J. Wu, *Nano Research* **12** (2019) 77.
70. Arramel, P. Hu, A. Xie, X. Yin, C. S. Tang, K. Ikeda, M. H. Mahyuddin, M. F. Sahdan, D. Wang, K. Yoshizawa, H. Wang, M. D. Birowosuto, C. Dang, A. Rusydi, A. T. S. Wee and J. Wu, *J. Mater. Chem. C* **8** (2020) 12587.
71. P. Schulz, L. L. Whittaker-Brooks, B. A. MacLeod, D. C. Olson, Y.-L. Loo and A. Kahn, *Advanced Materials Interfaces* **2** (2015) 1400532.
72. X. Zhang, Z. Su, B. Zhao, Y. Yang, Y. Xiong, X. Gao, D.-C. Qi and L. Cao, *Applied Physics Letters* **113** (2018) 113901.
73. Y. Lin, B. Chen, F. Zhao, X. Zheng, Y. Deng, Y. Shao, Y. Fang, Y. Bai, C. Wang and J. Huang, *Advanced Materials* **29** (2017) 1700607.
74. A. M. Boehm, T. Liu, S. M. Park, A. Abtahi and K. R. Graham, *ACS Applied Materials & Interfaces* **12** (2020) 5209.
75. N. K. Noel, A. Abate, S. D. Stranks, E. S. Parrott, V. M. Burlakov, A. Goriely and H. J. Snaith, *ACS Nano* **8** (2014) 9815.
76. X. Zheng, B. Chen, J. Dai, Y. Fang, Y. Bai, Y. Lin, H. Wei, X. C. Zeng and J. Huang, *Nature Energy* **2** (2017) 17102.
77. F. Zu, P. Amsalem, M. Ralaiarisoa, T. Schultz, R. Schlesinger and N. Koch, *ACS Applied Materials & Interfaces* **9** (2017) 41546.
78. E. E. Perry, J. G. Labram, N. R. Venkatesan, H. Nakayama and M. L. Chabinyc, *Advanced Electronic Materials* **4** (2018) 1800087.
79. L. Zhao, Y. L. Lin, H. Kim, N. C. Giebink and B. P. Rand, *ACS Energy Letters* **3** (2018) 2708.
80. J. V. Passarelli, C. M. Mauck, S. W. Winslow, C. F. Perkinson, J. C. Bard, H. Sai, K. W. Williams, A. Narayanan, D. J. Fairfield, M. P. Hendricks, W. A. Tisdale and S. I. Stupp, *Nature Chemistry* **12** (2020) 672.
81. K. Leng, L. Wang, Y. Shao, I. Abdelwahab, G. Grinblat, I. Verzhbitskiy, R. Li, Y. Cai, X. Chi, W. Fu, P. Song, A. Rusydi, G. Eda, S. A. Maier and K. P. Loh, *Nature Communications* **11** (2020) 5483.
82. G. Liu, X.-X. Xu, S. Xu, L. Zhang, H. Xu, L. Zhu, X. Zhang, H. Zheng and X. Pan, *J. Mater. Chem. A* **8** (2020) 5900.
83. X. Zhang, X. Ren, B. Liu, R. Munir, X. Zhu, D. Yang, J. Li, Y. Liu, D.-M. Smilgies, R. Li, Z. Yang, T. Niu, X. Wang, A. Amassian, K. Zhao and S. F. Liu, *Energy Environ. Sci.* **10** (2017) 2095.
84. B.-E. Cohen, Y. Li, Q. Meng and L. Etgar, *Nano Letters* **19** (2019) 2588.
85. J. Hu, I. W. H. Oswald, S. J. Stuard, M. M. Nahid, N. Zhou, O. F. Williams, Z. Guo, L. Yan, H. Hu, Z. Chen, X. Xiao, Y. Lin, Z. Yang, J. Huang, A. M. Moran, H. Ade, J. R. Neilson and W. You, *Nature Communications* **10** (2019) 1276.
86. D. H. Cao, C. C. Stoumpos, O. K. Farha, J. T. Hupp and M. G. Kanatzidis, *Journal of the American Chemical Society* **137** (2015) 7843.
87. B. Sun, Y. Xu, Y. Chen and W. Huang, *APL Materials* **8** (2020) 040901.
88. J. Wang, H. Zhang, L. Wang, K. Yang, L. Cang, X. Liu and W. Huang, *ACS Applied Energy Materials* **3** (2020) 4484.
89. M. M. Tavakoli, K.-H. Tsui, Q. Zhang, J. He, Y. Yao, D. Li and Z. Fan, *ACS Nano* **9** (2015) 10287.

90. A. Xie, F. Maddalena, M. E. Witkowski, M. Makowski, B. Mahler, W. Drozdowski, S. V. Springham, P. Coquet, C. Dujardin, M. D. Birowosuto and C. Dang, *Chemistry of Materials* **32** (2020) 8530.
91. E. R. Dohner, A. Jaffe, L. R. Bradshaw and H. I. Karunadasa, *J Am Chem Soc* **136** (2014) 13154.
92. D. Cortecchia, S. Neutzner, A. R. Srimath Kandada, E. Mosconi, D. Meggiolaro, F. De Angelis, C. Soci and A. Petrozza, *Journal of the American Chemical Society* **139** (2017) 39.
93. D. Cortecchia, J. Yin, A. Bruno, S.-Z. A. Lo, G. G. Gurzadyan, S. Mhaisalkar, J.-L. Brédas and C. Soci, *J. Mater. Chem. C* **5** (2017) 2771.
94. T. Sheikh, A. Shinde, S. Mahamuni and A. Nag, *ACS Energy Letters* **3** (2018) 2940.
95. Q. Shan, C. Wei, Y. Jiang, J. Song, Y. Zou, L. Xu, T. Fang, T. Wang, Y. Dong, J. Liu, B. Han, F. Zhang, J. Chen, Y. Wang and H. Zeng, *Light: Science & Applications* **9** (2020) 163.
96. J. Y. Kim, J.-W. Lee, H. S. Jung, H. Shin and N.-G. Park, *Chemical Reviews* **120** (2020) 7867, pMID: 32786671.
97. X.-K. Liu, W. Xu, S. Bai, Y. Jin, J. Wang, R. H. Friend and F. Gao, *Nature Materials* .
98. T. M. Koh, V. Shanmugam, J. Schlipf, L. Oesinghaus, P. Müller-Buschbaum, N. Ramakrishnan, V. Swamy, N. Mathews, P. P. Boix and S. G. Mhaisalkar, *Advanced Materials* **28** (2016) 3653.
99. P. Gao, M. Grätzel and M. K. Nazeeruddin, *Energy Environ. Sci.* **7** (2014) 2448.
100. S. Chen and G. Shi, *Advanced Materials* **29** (2017) 1605448.
101. J. Jagielski, S. Kumar, W.-Y. Yu and C.-J. Shih, *J. Mater. Chem. C* **5** (2017) 5610.
102. Y. Chen, Y. Sun, J. Peng, J. Tang, K. Zheng and Z. Liang, *Advanced Materials* **30** (2018) 1703487.
103. I. C. Smith, E. T. Hoke, D. Solis-Ibarra, M. D. McGehee and H. I. Karunadasa, *Angewandte Chemie International Edition* **53** (2014) 11232.
104. T. He, S. Li, Y. Jiang, C. Qin, M. Cui, L. Qiao, H. Xu, J. Yang, R. Long, H. Wang and M. Yuan, *Nature Communications* **11** (2020) 1672.
105. M. Wei, K. Xiao, G. Walters, R. Lin, Y. Zhao, M. I. Saidaminov, P. Todorović, A. Johnston, Z. Huang, H. Chen, A. Li, J. Zhu, Z. Yang, Y.-K. Wang, A. H. Proppe, S. O. Kelley, Y. Hou, O. Voznyy, H. Tan and E. H. Sargent, *Advanced Materials* **32** (2020) 1907058.
106. S. Gharibzadeh, I. M. Hossain, P. Fassl, B. A. Nejand, T. Abzieher, M. Schultes, E. Ahlswede, P. Jackson, M. Powalla, S. Schäfer, M. Rienäcker, T. Wietler, R. Peibst, U. Lemmer, B. S. Richards and U. W. Paetzold, *Advanced Functional Materials* **30** (2020) 1909919.
107. G. Grancini, C. Roldán-Carmona, I. Zimmermann, E. Mosconi, X. Lee, D. Martineau, S. Narbey, F. Oswald, F. De Angelis, M. Graetzel and M. K. Nazeeruddin, *Nature Communications* **8** (2017) 15684.
108. J. Sun, N. Chandrasekaran, C. Liu, A. D. Scully, W. Yin, C. K. Ng and J. J. Jasieniak, *ACS Applied Energy Materials* **3** (2020) 8205.
109. N. K. Noel, S. D. Stranks, A. Abate, C. Wehrenfennig, S. Guarnera, A.-A. Haghighirad, A. Sadhanala, G. E. Eperon, S. K. Pathak, M. B. Johnston, A. Petrozza, L. M. Herz and H. J. Snaith, *Energy & Environmental Science* **7** (2014) 3061.
110. C. Ma, D. Shen, T.-W. Ng, M.-F. Lo and C.-S. Lee, *Advanced Materials* **30** (2018) 1800710.
111. C. Zhou, W. Chen, S. Yang, Q. Ou, Z. Gan, Q. Bao, B. Jia and X. Wen, *ACS Applied Materials & Interfaces* **12** (2020) 26384.
112. N. Zhou, Y. Shen, L. Li, S. Tan, N. Liu, G. Zheng, Q. Chen and H. Zhou, *Journal of the American Chemical Society* **140** (2018) 459.
113. T. Wu, Y. Wang, X. Li, Y. Wu, X. Meng, D. Cui, X. Yang and L. Han, *Advanced Energy Materials* **9** (2019) 1803766.
114. Q. Jiang, Y. Zhao, X. Zhang, X. Yang, Y. Chen, Z. Chu, Q. Ye, X. Li, Z. Yin and J. You, *Nature Photonics* **13** (2019) 460.
115. S. M. Park, A. Abtahi, A. M. Boehm and K. R. Graham, *ACS Energy Letters* **5** (2020) 799.
116. Z.-K. Wang and L.-S. Liao, *Advanced Optical Materials* **6** (2018) 1800276.
117. L. Yangi, Y. Li, Y. Pei, J. Wang, H. Lin and X. Li, *J. Mater. Chem. A* **8** (2020) 7808.
118. A. Krishna, S. Gottis, M. K. Nazeeruddin and F. Sauvage, *Advanced Functional Materials* **29** (2019) 1806482.
119. L. Zhou, Z. Lin, Z. Ning, T. Li, X. Guo, J. Ma, J. Su, C. Zhang, J. Zhang, S. Liu, J. Chang and Y. Hao, *Solar RRL* **3** (2019) 1900293.
120. M.-c. Kim, S.-Y. Ham, D. Cheng, T. A. Wynn, H. S. Jung and Y. S. Meng, *Advanced Energy Materials* **n/a** (2020) 2001753.
121. M. Yuan, L. N. Quan, R. Comin, G. Walters, R. Sabatini, O. Voznyy, S. Hoogland, Y. Zhao, E. M. Beauregard, P. Kanjanaboos, Z. Lu, D. H. Kim and E. H. Sargent, *Nature Nanotechnology* **11** (2016) 872.
122. N. Wang, L. Cheng, R. Ge, S. Zhang, Y. Miao, W. Zou, C. Yi, Y. Sun, Y. Cao, R. Yang, Y. Wei, Q. Guo, Y. Ke, M. Yu, Y. Jin, Y. Liu, Q. Ding, D. Di, L. Yang, G. Xing, H. Tian, C. Jin, F. Gao, R. H. Friend, J. Wang and W. Huang, *Nature Photonics* **10** (2016) 699.
123. X. Yang, X. Zhang, J. Deng, Z. Chu, Q. Jiang, J. Meng, P. Wang, L. Zhang, Z. Yin and J. You, *Nature Communications* **9** (2018) 570.
124. J. Xing, Y. Zhao, M. Askerka, L. N. Quan, X. Gong, W. Zhao, J. Zhao, H. Tan, G. Long, L. Gao, Z. Yang, O. Voznyy, J. Tang, Z.-H. Lu, Q. Xiong

and E. H. Sargent, *Nature Communications* **9** (2018) 3541.
125. G. Li, F. W. R. Rivarola, N. J. L. K. Davis, S. Bai, T. C. Jellicoe, F. de la Peña, S. Hou, C. Ducati, F. Gao, R. H. Friend, N. C. Greenham and Z.-K. Tan, *Advanced Materials* **28** (2016) 3528.
126. L. N. Quan, Y. Zhao, F. P. García de Arquer, R. Sabatini, G. Walters, O. Voznyy, R. Comin, Y. Li, J. Z. Fan, H. Tan, J. Pan, M. Yuan, O. M. Bakr, Z. Lu, D. H. Kim and E. H. Sargent, *Nano Letters* **17** (2017) 3701.
127. S. Kumar, J. Jagielski, S. Yakunin, P. Rice, Y.-C. Chiu, M. Wang, G. Nedelcu, Y. Kim, S. Lin, E. J. G. Santos, M. V. Kovalenko and C.-J. Shih, *ACS Nano* **10** (2016) 9720.
128. Q. Wang, J. Ren, X.-F. Peng, X.-X. Ji and X.-H. Yang, *ACS Applied Materials & Interfaces* **9** (2017) 29901.
129. Z. Chen, C. Zhang, X.-F. Jiang, M. Liu, R. Xia, T. Shi, D. Chen, Q. Xue, Y.-J. Zhao, S. Su, H.-L. Yip and Y. Cao, *Advanced Materials* **29** (2017) 1603157.
130. D. N. Congreve, M. C. Weidman, M. Seitz, W. Paritmongkol, N. S. Dahod and W. A. Tisdale, *ACS Photonics* **4** (2017) 476.
131. L. Cheng, Y. Cao, R. Ge, Y.-Q. Wei, N.-N. Wang, J.-P. Wang and W. Huang, *Chinese Chemical Letters* **28** (2017) 29 .